# Effect of molecular functionality on the photocatalytic oxidation of gas-phase mixtures

Michael E. Zorn [a,*], Stephen O. Hay [b], Marc A. Anderson [c]

[a] Department of Natural and Applied Sciences (Chemistry), University of Wisconsin-Green Bay, 2420 Nicolet Drive, Green Bay, WI 54311, United States
[b] Physical Sciences Department, United Technologies Research Center, 411 Silver Lane, East Hartford, CT 06108, United States
[c] Environmental Chemistry and Technology Program, University of Wisconsin-Madison, 660 North Park Street, Madison, WI 53706, United States

## ARTICLE INFO

## ABSTRACT

Developing an effective air purifier for indoor air quality (IAQ) purposes requires knowledge of the reaction rate of target compounds in the presence of other compounds that compete favorably with the target compounds for surface sites. To address this issue, the photocatalytic oxidation (PCO) of five C3 organic compounds on a sol-gel derived $TiO_2$ thin-film catalyst was examined. Photocatalytic degradation of the five compounds was first compared in single component experiments at 50% relative humidity. The photocatalytic oxidation reaction rates proceeded in the following order: 1-propanol > propanal > propanone > propene > propane. The order of reaction rates was partially explained by considering the intermolecular forces of attraction that exist between the gas-phase molecules and the hydrated titania surface, with the lone exception of the ketone. A model that incorporates Henry's law constant and hydroxyl radical reactivity was successful at predicting PCO reactivity. Relative photocatalytic degradation was also studied using multi-component experiments. Multi-component experiments with propanone + propene, propanal + propanone, and ethanol + propanone were conducted. In each case it was observed that compounds with stronger binding energy to the photocatalyst surface displaced compounds with weaker binding energies and inhibited their further reaction until the stronger binding species was oxidized to sufficiently low levels. Further investigation of relative binding energies of compounds of interest for PCO applications should be pursued in the future through combinations of experimental studies and theoretical molecular modeling techniques.

© 2010 Elsevier B.V. All rights reserved.

## 1. Introduction

Photocatalysis is an interesting phenomenon that has been vigorously pursued in both industrial and academic environs over the last several decades [1–8]; it was reported as long ago as 1964 [9]. This is due, in large part, to the potential for mineralizing trace contaminants in both air and water to innocuous products (e.g., $CO_2$ and $H_2O$). A plethora of air and water purifiers based on photocatalytic technology have been developed, deployed as prototypes in various environments, and marketed throughout Japan, Europe, and North America. Claims on the performance of these products are rarely realized in practice, since there exists a lack of fundamental understanding of the photocatalytic process, which results in the inability to predict reactor (purifier) performance in a real-world environment.

Our joint interest in photocatalysis arises from the application of this technology to Indoor Air Quality (IAQ) improvement. Developing an effective air purifier for IAQ purposes requires the ability to predict the performance of the device over the range of variability of the appropriate atmospheric variables (e.g., temperature, humidity, species, and concentration) and design variables (e.g., flow rate, light intensity distribution, and catalyst surface area). This means that one needs to measure or estimate rate constants for the photocatalytic oxidation (PCO) of the primary contaminants of interest over the expected range of concentrations and atmospheric conditions for the catalyst of choice and in the range of light intensity of choice. Furthermore, one needs to understand what the effect of mixing all these species into one atmospheric soup has on the individual rates.

Several groups have measured PCO removal rates of single contaminant species [10–12] and mixtures [13–19] that are important to IAQ. Several of these studies showed a correlation between molecular functionality, structure, and/or properties and PCO removal rates. For example, Obee and Hay [14] demonstrated oxidation rates for C4 species in the order: 1-butanol > 2-butanone > 1-butene > *n*-butane and hypothesized that the ranking followed the order of intermolecular forces attracting the gas-phase species to the polar catalyst surface. They further showed that PCO

rates increased with molecular mass for alkanes. This is consistent with the expected increase in London forces. They hypothesized that the hierarchy of intermolecular forces of attraction between the gas-phase molecules and the polar partially hydroxylated titania surface could be used to both explain the observed rates and predict the PCO rates for species that had not been measured in the laboratory.

Hodgson et al. [19] studied PCO removal rates in a prototype reactor of a 27 compound mixture to simulate an indoor air environment. Their observed oxidation rates of (represented) chemical classes followed the approximate order of alcohols and glycol ethers > aldehydes, ketones, and terpene hydrocarbons > aromatic and alkane hydrocarbons > halogenated hydrocarbons. Their results are consistent with Obee and Hay [14] and with the results reported in this paper. They attempted to correlate their conversion efficiency with a variety of parameters including: Henry's law constant, octanol-water partition coefficient, vapor pressure, aqueous solubility, and gas-phase reaction rates with hydroxyl radicals; correlation with Henry's law constant was found to be the single most accurate descriptor. They hypothesized that in their observed humidity range (42–65% RH), physisorbed water on the surface would be expected to be on the order of ca. 2 monolayers [20], and that interaction of the gas-phase molecules with the catalyst surface could be related to gas dissolving into aqueous solution. In this humidity range, the photocatalyst surface contains a significant amount of physisorbed water, and only about 3–5% of the water is hydrogen bonded or chemisorbed [19,21].

It is apparent from these studies that PCO rate constants are related to the forces of attraction between gas-phase molecules and the catalyst surface and that there is significant competition for adsorption on the catalyst surface between all the components in the gas phase. The exact nature of the catalyst surface depends on the photocatalyst composition, the crystalline phase, the surface morphology, the extent of chemisorptions, and so on. Physisorption on the surface depends on the concentration of the various species in the gas phase and the nature of the surface. At low concentrations, species may be expected to react independently of each other; however, at higher concentrations, the species that dominate the surface would be expected to dictate reaction rates.

The study reported here is concerned with the PCO removal rates of C3 species separately and in a mixture using a recirculating reactor. Utilization of a recirculating reactor has several advantages over reactors that employ a single-pass approach where the contaminant feed stream only passes through the reactor once. First, an entire kinetic data set can be obtained with a single experiment (generally lasting only a few hours or less) using the recirculating design. Conversely, a single-pass approach requires numerous readjustments of the flow rate to catalyst ratio, followed by measurement of degradation, to yield a sufficient number of data points required for a kinetic analysis. Therefore, the time required for single-pass kinetic studies is significantly larger than with a recirculating design. A second major advantage of using a recirculating design is that multiple compounds can be introduced into the system to directly study the co-adsorption interference effects of different chemical classes, as was done in this study.

## 2. Experimental

### 2.1. Catalyst preparation

Stable sols of titanium dioxide ($TiO_2$) nanoparticles were prepared according to the method of Xu and Anderson [22]. In this method, titanium tetra-isopropoxide $Ti\{OCH(CH_3)_2\}_4$ (Aldrich, Milwaukee, WI) was subjected to an acidic hydrolysis by addition to
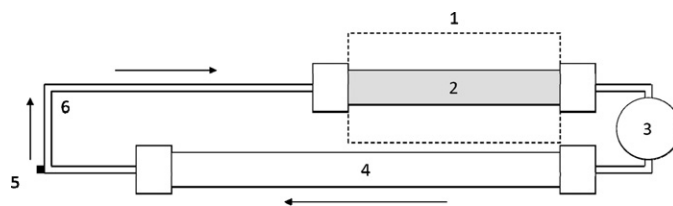


**Fig. 1.** Recirculating reactor design. 1 – temperature-controlled chamber with two UV light sources; 2 – illuminated glass tube randomly packed with 30 catalyst-coated glass rings; 3 – recirculating pump; 4 – non-illuminated empty glass tube (not packed with catalyst-coated glass rings); 5 – sampling port (septum); 6 – stainless steel tubing.

an aqueous solution of nitric acid. The volumetric mixing ratio was 1 $HNO_3$:136.4 $H_2O$:11.4 $Ti\{OCH(CH_3)_2\}_4$. The resulting $TiO_2$ precipitate was peptized at room temperature for 3 days resulting in a stable sol. This acidic sol was then dialyzed for 3 days using a dialysis membrane (Spectra/Por® 3 membrane, 3500 MW cutoff, Spectrum, Laguna Hills, CA) to a final pH of 3.5. Three layers of active catalyst material were deposited onto borosilicate glass cylinders or "rings" (5 mm o.d. × 3 mm i.d. × 10 mm long) that were pre-cleaned prior to coating. The coatings were applied by dipping the rings in the sol and then withdrawing at a rate of 30 cm/min. After applying each layer, the rings were dried in air at 120 °C for 1 h. The coated rings were then fired in air in a furnace at 350 °C for 3 h using a ramp rate of 1 °C/min.

The mass of catalyst used in this study was measured by digesting a subsample of catalyst-coated rings in hot acid, followed by determination of titanium by inductively coupled plasma atomic emission spectroscopy (ICP-AES). The previously reported digestion procedure [7,23–25] involved adding ~4 g of ammonium sulfate [$(NH_4)_2SO_4$] to 10 mL of hot concentrated sulfuric acid ($H_2SO_4$). After the $(NH_4)_2SO_4$ completely dissolved in the $H_2SO_4$, five catalyst-coated glass rings were added to the solution. The sample was then covered and carefully boiled for 1 h. The acidic solution containing the digested catalyst was diluted to 25 mL with ultra-high purity water; 3 mL of the concentrated solution was then further diluted to 100 mL using ultra-high purity water. Visual inspection of the digested rings suggests that the digestion process completely removed all of the catalyst coating. The sample was analyzed for titanium by ICP-AES using a Varian Liberty Series II Sequential ICP (Varian, Inc., Palo Alto, CA). The total mass of catalyst deposited on each ring was determined to be 0.23 mg $TiO_2$.

### 2.2. Reactor apparatus

The photocatalytic oxidation experiments employed a recycling loop as shown in Fig. 1. The recycling loop consisted of a temperature-controlled chamber containing two 4 W fluorescent UV light sources (F4T5BL, EIKO Brand, Bulb Direct Co., Pittsford, NY), a 29 mL glass tube (1.5 cm i.d. × 16.5 cm long) that held 30 catalyst-coated glass rings packed randomly in the center, a non-illuminated 53 mL empty glass tube (1.5 cm i.d. × 30.5 cm long) to add additional volume to the loop, a sampling port (septum), stainless steel tubing, and a recirculating diaphragm pump with chemically inert components (Model UNMP-30 modified with PTFE-coated diaphragm and Kalrez valves and seals, KNF Neuberger, Inc, Trenton, NJ). The total mass of catalyst was $6.9 \times 10^{-3}$ g and the void volume of the reaction loop was 100 mL. By suitable adjustment of a cooling air stream, the reactor air temperature (measured by placing a J-type thermocouple in a glass insert located at the center of the packed bed) was maintained at a temperature of 30 °C. The two fluorescent light bulbs were spaced at opposite sides (at a radius of 2.5 cm from the centerline) of the glass tube containing the catalyst-coated glass rings. These bulbs produced a strong peak cen-

tered at ca. 365–370 nm and provided an average measured light irradiance of $1.6\,MW\,cm^{-2}$. Light irradiance measurements were made by inserting a radiometer (Model IL 1400 with Super-Slim probe, International Light, Newburyport, MA) into the reactor housing after removal of the catalyst-containing glass tube. The reported value is an average of 5 separate irradiance measurements.

For most experiments, the UV lights were energized, the reactor temperature was allowed to reach the set temperature of 30 °C, the recycling loop was opened, and the entire loop was flushed with ultra zero air (<0.1 ppm total hydrocarbons, <5 ppm water vapor, AGA Specialty Gas, Cleveland, OH) that was preconditioned to 50% relative humidity. The relative humidity exiting the opened reaction loop was measured with a calibrated humidity meter (Model HM 34, Vaisala, Woburn, MA). After flushing with 50% relative humidity air for 15 min, the air flow was stopped, the loop was closed, and the pump was started. Test compounds were then introduced into the reaction system through the sampling port. Gas samples (50 μL) were withdrawn from the recycling loop at regular intervals by inserting a gastight syringe through the sampling port.

### 2.3. Gas chromatography

The reactor contents were analyzed using a Hewlett-Packard 5890 Series II gas chromatograph with a mass selective detector, GC-MSD. Helium was used as the carrier gas. As mentioned above, a 50 μL injection was performed using a gastight syringe. The injector was operated in the split mode with a split ratio of 40:1. The GC column was an HP-5 capillary column (25 m long × 0.2 mm i.d. × 0.33 μm film thickness, Agilent Technologies, Santa Clara, CA) that was maintained at 35 °C for 3 min. The injection port temperature was 250 °C and the MSD transfer line was maintained at 280 °C. The MSD was operated in the selected ion monitoring (SIM) mode to increase the sensitivity for target compounds. The following $m/z$ values were used to quantify each of the target compounds: carbon dioxide ($m/z = 44$), propane ($m/z = 44$), propene ($m/z = 42$), propanal ($m/z = 58$), propanone ($m/z = 43$), and 1-propanol ($m/z = 31$).

### 2.4. Kinetics

To allow estimation of kinetic rate constants, the concentration of each compound was measured over time. The data generated in this study were fit according to a general power law model, with a reaction rate expression of the form:

$$r_A = -kC_A^n \qquad (1)$$

where $r_A$ is the analyte reaction rate (in units of $mol\,g^{-1}\,s^{-1}$), $k$ is the reaction rate constant (units depend on the reaction order, $n$), and $C_A$ is the analyte concentration (in units of $mol\,L^{-1}$). The conversion data generated in this study were initially fit using ½ order and 1st order reaction rate models. The best fit kinetic model ranged from ½ order to 1st order depending on the analyte; therefore, a 3/4 order model was applied to all data sets to allow for comparison of reaction rate constants between compounds.

A linearized form of a 3/4 order model can be written as:

$$C_A^{1/4} = C_{A0}^{1/4} - \frac{ktW}{4V} \qquad (2)$$

where $C_A$ is the concentration of the analyte (in units of $mol\,L^{-1}$) at a given time ($t$, in units of s), $C_{A0}$ is the initial concentration of the analyte, $k$ is the reaction rate constant (in units of $mol^{0.25}\,L^{0.75}\,g^{-1}\,s^{-1}$), $W$ is the catalyst mass (in units of g), and $V$ is the void volume of the reactor (in units of L) – see Hill [26] for a detailed discussion of kinetic modeling. The reaction rate constant can be determined by performing a least squares regression analysis of $C_A^{1/4}$ versus time,
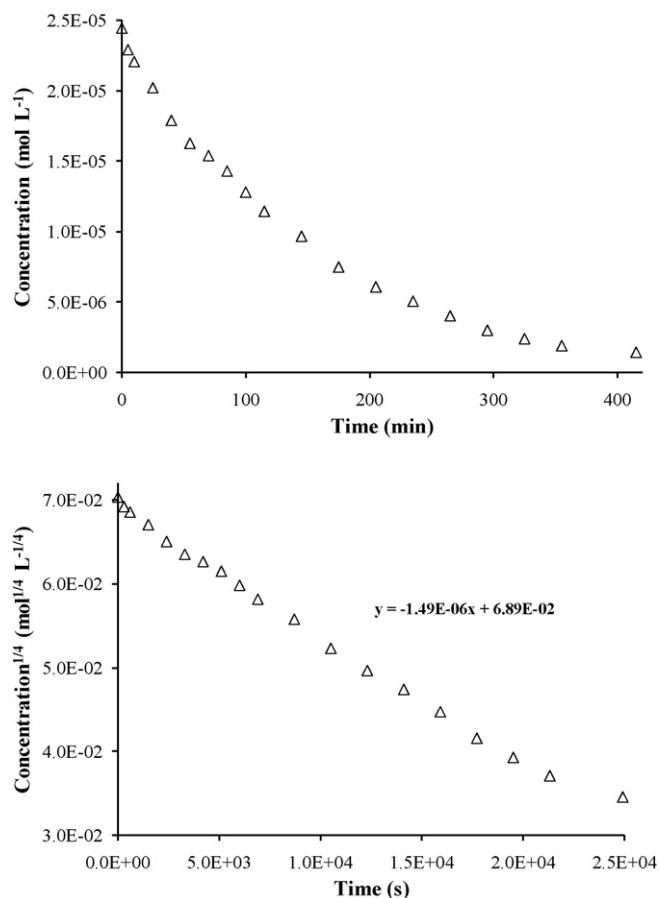


**Fig. 2.** Top: Propane concentration versus time during a photocatalysis reaction at 30 °C and 50% relative humidity. Bottom: Fit of the propane conversion data to a linearized 3/4 order kinetic model.

where the reaction rate constant is calculated as:

$$k = -\frac{\text{slope }4V}{W} \qquad (3)$$

The 3/4 order model (i.e. $n = 0.75$) can be explained as being the apparent order resulting from the Langmuir–Hinshelwood–Hougen–Watson mechanism with the coverage $\theta$, varying as $\theta = K_A C_A/(1 + K_A C_A)$ where $K_A$ is the constant for adsorption of the analyte onto the surface of the catalyst. In a rather narrow range of concentrations, the homographic function $\theta = K_A C_A/(1 + K_A C_A)$ can be closely approximated by a power function as:

$$r_A = -k\theta = -\frac{kK_A C_A}{1 + K_A C_A} = -k\,C_A^n \qquad (4)$$

## 3. Results and discussion

### 3.1. Single component experiments

Single component photocatalysis experiments were performed on five different three-carbon atom-containing compounds with different functionality (likely leading to different affinity for the catalyst surface). The compounds were propane, propene, propanal (a.k.a.: propionaldehyde), propanone (a.k.a.: acetone), and 1-propanol. The degradation of each compound was measured over time at 50% relative humidity using a sol-gel based $TiO_2$ thin-film catalyst in the presence of UV light at a temperature of 30 °C.

Figs. 2–6 show the kinetic data for each of these compounds. The top graph in each figure depicts the experimental concentration (in
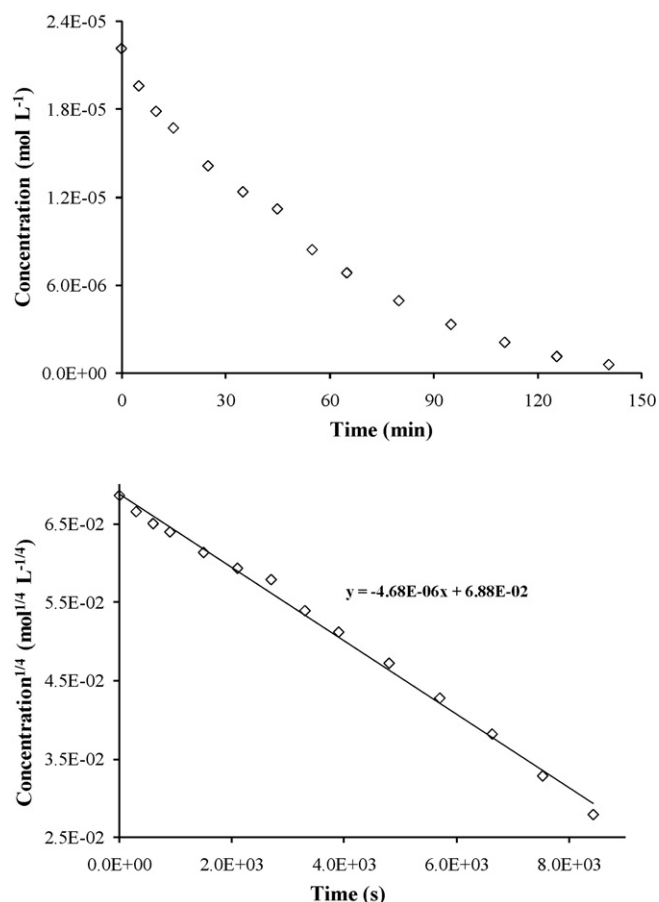
**Fig. 3.** Top: Propene concentration versus time during a photocatalysis reaction at 30 °C and 50% relative humidity. Bottom: Fit of the propene conversion data to a linearized 3/4 order kinetic model.
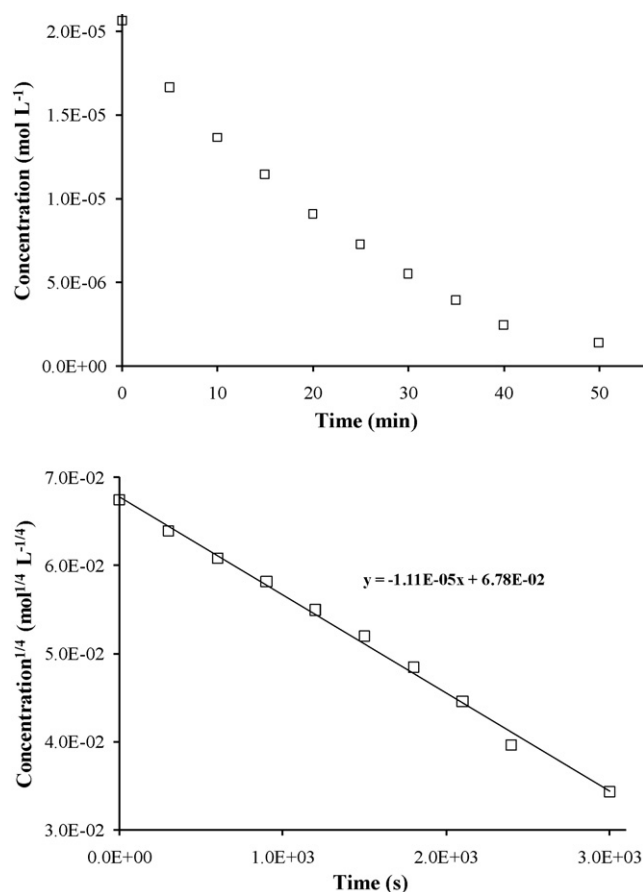


**Fig. 4.** Top: Propanone concentration versus time during a photocatalysis reaction at 30 °C and 50% relative humidity. Bottom: Fit of the propanone conversion data to a linearized 3/4 order kinetic model.

units of $mol\,L^{-1}$) versus time, while the bottom graph in each figure depicts the linearized 3/4 order form of the data, as given in Eq. (2). Conversions between $mol\,L^{-1}$ and ppmv were done using an ambient temperature of 25 °C and pressure of 1 atm. As shown, the 3/4 order model provides a reasonable fit to the data for each compound. Fig. 7 summarizes the five data sets on a single graph to allow for comparison of their relative reactivity in *single component* experiments. The time corresponding to a concentration of ~$1.1 \times 10^{-5}\,mol\,L^{-1}$ (270 ppmv) is set to time zero for each compound to allow for a relevant comparison of the reactivity. The solid lines represent the predicted concentration at each time using the calculated reaction rate constants (see below) along with Eq. (2). As shown, 1-propanol reacted the fastest, followed by propanal, propanone, propene, and then propane.

The generation of carbon dioxide also was monitored to calculate a mass balance of carbon during each photocatalysis experiment. Each of the compounds studied should produce 3 moles of carbon dioxide per mole degraded, according to stoichiometry. Only propane and propene yielded mineralization ratios below 3; the mineralization ratios for these two compounds were 2.9 and 2.8, respectively. This indicates that the test compounds were completely mineralized to carbon dioxide and water throughout the course of the reactions. This also provides evidence that there were no significant leaks in the reaction loop.

The linearized 3/4 order kinetic model was used to calculate a kinetic rate constant for each of the five compounds. The 3/4 order rate constants are listed in Table 1. 1-Propanol has the largest reaction rate constant, followed by propanal, propanone, propene, and then propane. As expected, the calculated rate con-

stants are consistent with the relative reactivity data presented in Fig. 7.

If we relate the relative rates of reaction to the intermolecular forces of attraction between the molecules and the surface, we would predict that hydrogen bonding would dominate and that dipole-dipole interactions would be next dominant for molecules of similar molecular mass. We do observe that the alcohol, which can hydrogen bond to the hydrated titania surface, disappears in ca. half the time as the next fastest species studied (see Fig. 7). Differences in molecular polarity could provide a partial explanation for the difference in observed reactivity of the other four compounds. Since the surface of the catalyst is polar, and it would contain a significant amount of bound water at 50% relative humidity, compounds with greater polarity would be expected to preferentially adsorb to the surface and, therefore, react faster than less polar compounds. To test this hypothesis, the calculated reaction rate constants were plotted versus the dipole moment (i.e., polarity) of the compounds (see Fig. 8). As shown, the relative reactivity of propane, propene, and propanal are well explained by the dipole moment. In fact, there is a linear relationship between reaction rate constant and the dipole moment for these three compounds.

Propanone and 1-propanol, however, do not follow this trend. The increased reactivity of 1-propanol can be explained, as previously mentioned, by the ability of this molecule to hydrogen bond to the catalyst surface. This would cause the adsorption (and therefore overall reactivity) of 1-propanol to be greater than predicted through polarity alone. Conversely, the reactivity of propanone is much lower than would be predicted by dipole moment alone. A second kinetic experiment was con-

**Table 1**
Experimental reaction rate constant ($k$), dipole moment, Henry's law constant ($K_H$), hydroxyl radical reaction rate constant ($k_{OH}$), predicted reaction rate constant using Eq. (5), and percent difference between experimental and predicted $k$ values.

| Compound | Expt. 3/4 order $k$ (mol$^{0.25}$ L$^{0.75}$ g$^{-1}$ s$^{-1}$) | Dipole moment (debyes)[a] | $K_H$ (mol kg$^{-1}$ bar$^{-1}$) | $k_{OH}$ (cm$^3$ molecule$^{-1}$ s$^{-1}$) | Pred. 3/4 order $k$ (mol$^{0.25}$ L$^{0.75}$ g$^{-1}$ s$^{-1}$) | Percent difference |
|---|---|---|---|---|---|---|
| Propane | $8.6 \times 10^{-5}$ | 0.084 | 0.0015[b] | $1.1 \times 10^{-12}$[c] | $8.6 \times 10^{-5}$ | 0.5 |
| Propene | $2.7 \times 10^{-4}$ | 0.366 | 0.0048[d] | $2.8 \times 10^{-11}$[e] | $2.6 \times 10^{-4}$ | 3 |
| Propanone | $6.5 \times 10^{-4}$ | 2.88 | 25[f] | $2.3 \times 10^{-13}$[e] | $6.7 \times 10^{-4}$ | 3 |
| Propanal | $1.6 \times 10^{-3}$ | 2.52 | 13[f] | $2.0 \times 10^{-11}$[e] | $1.8 \times 10^{-3}$ | 11 |
| 1-Propanol | $2.7 \times 10^{-3}$ | 1.68 | 160[g] | $5.5 \times 10^{-12}$[h] | $2.4 \times 10^{-3}$ | 10 |

[a] CRC Handbook of Chemistry and Physics [28].
[b] Wilhelm et al. [29].
[c] Atkinson et al. [30].
[d] Mackay and Shiu [31].
[e] Atkinson [27].
[f] Buttery et al. [32].
[g] Burnett [33].
[h] Atkinson et al. [34].

ducted for propanone to assess whether or not this data point was accurately determined. The second reaction rate constant was calculated to be $7.0 \times 10^{-4}$ mol$^{0.25}$ L$^{0.75}$ g$^{-1}$ s$^{-1}$ as compared to $6.5 \times 10^{-4}$ mol$^{0.25}$ L$^{0.75}$ g$^{-1}$ s$^{-1}$, a difference of only 7%. Both of these data points are plotted in Fig. 8.

This result is consistent with previously published studies [15,18]. Both Takeda et al. [15] and Zhang et al. [18] observed that propanal degrades faster than propanone on supported TiO$_2$ photocatalysts. In addition, both of these studies also performed separate adsorption experiments in the dark, and in both cases, the surface adsorption of propanal was greater than that of propanone. There is agreement between these results and the two-component mix-

ture testing results reported in the next section where it was also found that propanal preferentially adsorbed to the surface, since propanal inhibited propanone degradation.

It is possible to look beyond molecular polarity to explain the observed single component reactivity results. In a previous publication, Hodgson et al. [19] found that photocatalytic reaction rate constants were dependent on Henry's law constant ($K_H$) and the gas-phase reaction rate constant with hydroxyl radicals ($k_{OH}$). Their equation had the general form:

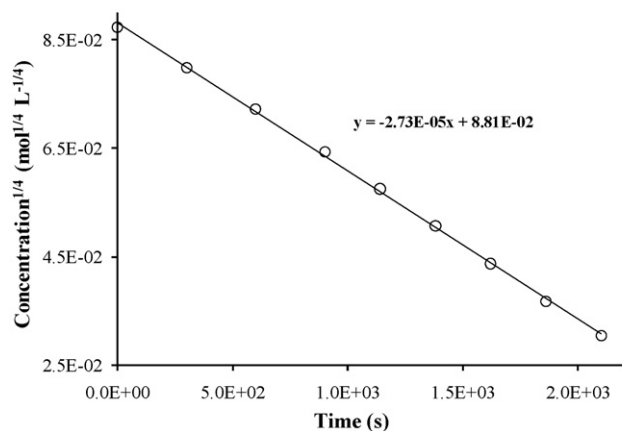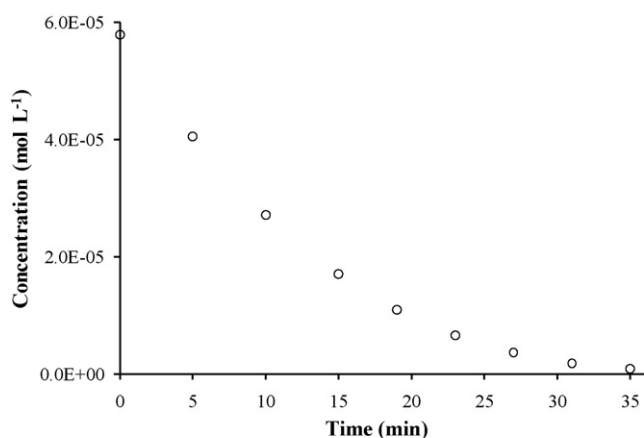$$\log k = a + b \log(K_H) + c \log(k_{OH}) \tag{5}$$



**Fig. 5.** Top: Propanal concentration versus time during a photocatalysis reaction at 30 °C and 50% relative humidity. Bottom: Fit of the propanal conversion data to a linearized 3/4 order kinetic model.
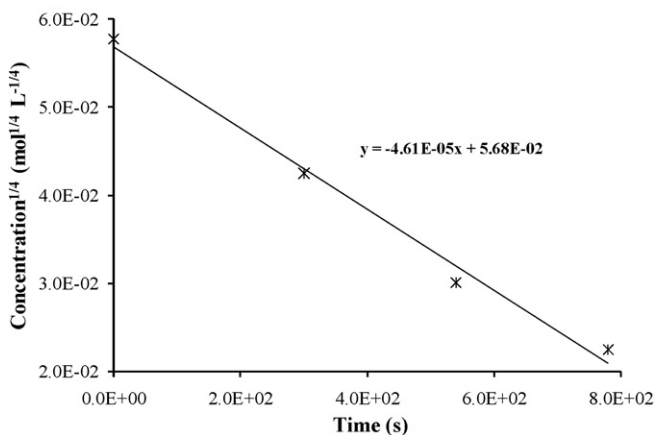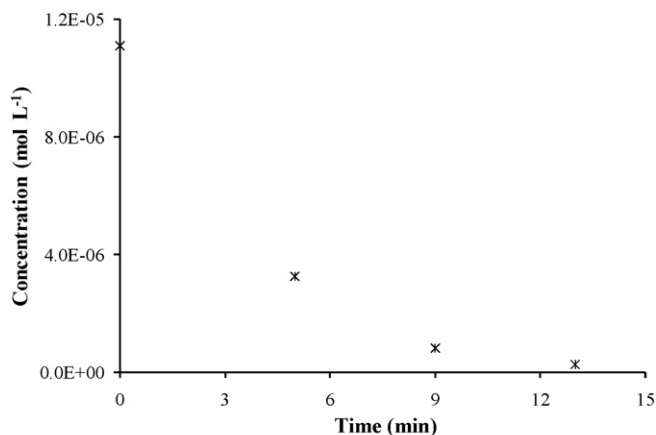


**Fig. 6.** Top: 1-Propanol concentration versus time during a photocatalysis reaction at 30 °C and 50% relative humidity. Bottom: Fit of the 1-propanol conversion data to a linearized 3/4 order kinetic model.
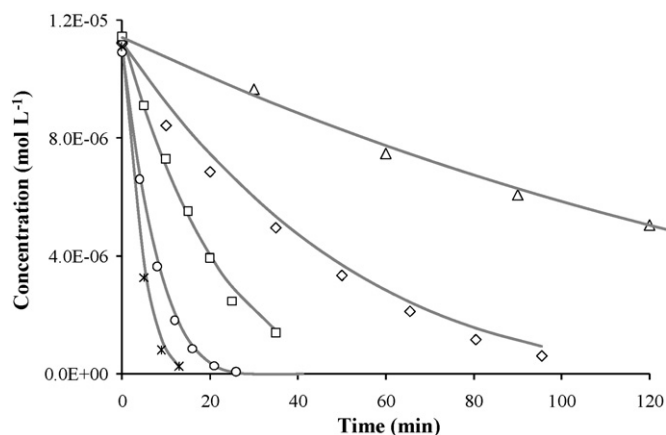
**Fig. 7.** Propane (△), propene (◇), propanone (□), propanal (◯), and 1-propanol (*) concentrations versus time during a photocatalysis reaction at 30 °C and 50% relative humidity. All four reactions were performed separately in *single component* experiments but are presented here on a single graph to allow for comparison of reactivity. The solid lines represent the predicted concentrations using the calculated reaction rate constants in Table 1 along with Eq. (2).

A similar regression was performed on the single component data generated in this study. Literature values for $K_H$ and $k_{OH}$ are listed in Table 1. The least squares regression parameters were found to be: $a = -0.3141$, $b = 0.2533$, and $c = 0.2539$. This method resulted in very good agreement between predicted and experimentally determined reaction rate constants. The predicted 3/4 order reaction rate constants are also listed in Table 1. Unlike polarity, this model predicts the relative reactivity of all five compounds. In fact, the model predicts the value of the reaction rate constants to within 3% for three of the compounds and to within 11% for the other two (percent difference values are also listed in Table 1).

### 3.2. Multi-component experiments

As mentioned above, a major advantage of using a recirculating design over a single-pass design is that multiple compounds can be introduced into the system to directly study the effects of competitive degradation. For example, if adsorption of reacting compounds to the surface is the rate limiting step, this allows direct comparison of the binding energies of similar species. Several different combinations of compounds were chosen to illustrate this concept. Propanone was the compound chosen for these multi-
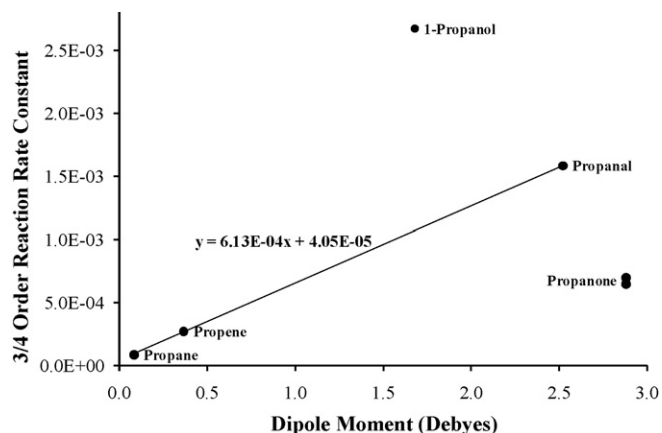


**Fig. 8.** Reaction rate constants (3/4 order) calculated for propane, propene, propanone, propanal, and 1-propanol from data obtained during single component photocatalysis reactions at 30 °C and 50% relative humidity. The propanone experiment was run twice for verification purposes.
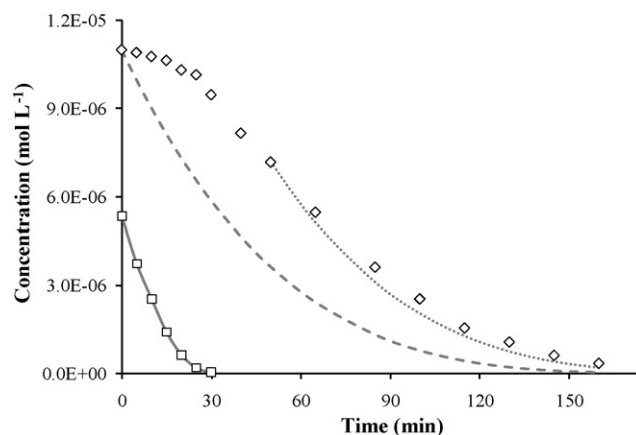


**Fig. 9.** Propene (◇) and propanone (□) concentrations versus time during a two-component photocatalysis reaction at 30 °C and 50% relative humidity. Both components were introduced into the reaction loop prior to energizing the light sources, which happened at time zero on the graph. The solid line represents the predicted propanone concentration using the calculated reaction rate constant in Table 1 along with Eq. (2). The dashed line represents the predicted concentration of propene from time zero. The dotted line represents the predicted concentration of propene after the propanone reached a sufficiently low concentration in the system. As shown, propene degradation is inhibited by the presence of propanone in this experiment.

component experiments due to its unusual behavior observed above and depicted in Fig. 8.

The first example of this type of experiment is shown in Fig. 9. In this experiment, two compounds (propene and propanone) were both introduced into the recirculating reaction system, and the concentrations were monitored over time. Both components were introduced into the reaction loop prior to energizing the light sources (time zero on the graph). In contrast to the reaction behavior shown in Fig. 3 where propene degradation began immediately, propene degradation was initially inhibited in this two-component system. Evidence of this effect is shown by the drastic difference in degradation rate before and after ca. 30 min. Before 30 min, propanone was present in the reactor at significant levels. Since propanone has a greater affinity for the catalyst surface (as given by dipole moment and Henry's law constant, see Table 1), propanone out-competed propene for surface sites, thereby limiting propene degradation. This is further illustrated by the dashed line, which represents the predicted concentration of propene from time zero. After 30 min, propanone was reduced to insignificant levels, allowing propene to react at an increased rate. This is shown by the dotted line, which represents the predicted concentration of propene after propanone reached a sufficiently low concentration in the system. It should be noted that this behavior cannot be predicted from the hydroxyl radical reactivity since propene has a larger $k_{OH}$ value than propanone (also listed in Table 1).

A second example is shown in Fig. 10. In this experiment, propanone was mixed with propanal. In this case, propanone degradation was initially inhibited by the presence of propanal. This is consistent with the results obtained in the single component experiments where propanal reacted faster than propanone. The results observed here suggest that propanal does in fact have a greater affinity for the catalyst surface and not just faster hydroxyl radical kinetics as postulated above. As mentioned, this is consistent with previously published studies that found that propanal reacted faster than propanone on supported TiO₂ and that the surface adsorption of propanal was greater than that of propanone [15,18]. Whatever the explanation, propanal inhibited the degradation of propanone in this experiment. Before ca. 10 min, propanal was present in the reactor at significant levels, which limited propanone degradation. As above, the dashed line represents the predicted
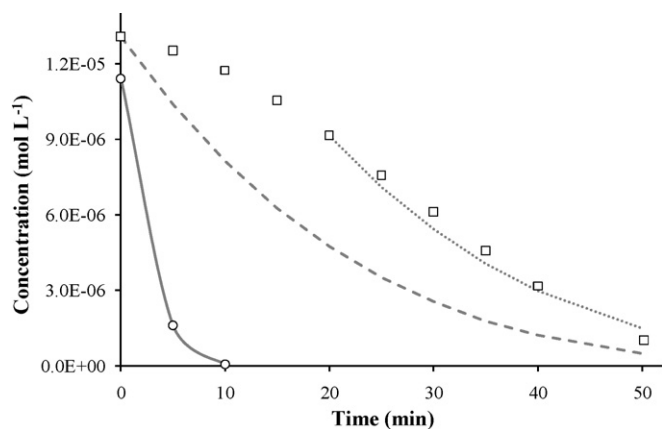
**Fig. 10.** Propanone (□) and propanal (○) concentrations versus time during a two-component photocatalysis reaction at 30 °C and 50% relative humidity. Both components were introduced into the reaction loop prior to energizing the light sources, which happened at time zero on the graph. The solid line represents the predicted propanal concentration using the calculated reaction rate constant in Table 1 along with Eq. (2). The dashed line represents the predicted concentration of propanone from time zero. The dotted line represents the predicted concentration of propanone after the propanal reached a sufficiently low concentration in the system. As shown, propanone degradation is inhibited by the presence of propanal in this experiment.

concentration of propanone from time zero. After 10 min, propanal was reduced to insignificant levels, allowing propanone to react at an increased rate. Again, the dotted line represents the predicted concentration of propanone after propanal reached a sufficiently low concentration in the system.

The two previous examples illustrate cases where two compounds were introduced simultaneously at the beginning of an experiment. The final example illustrates the effect of introducing an inhibiting compound into the reaction loop while another compound is in the process of reacting. In this example, propanone was spiked into the reaction loop at the beginning of the experiment. After a short period of time, ethanol (a compound that has the ability to hydrogen bond with the catalyst surface) was introduced into the loop. The results of this experiment are presented in Fig. 11. It should be noted that the recirculating reactor
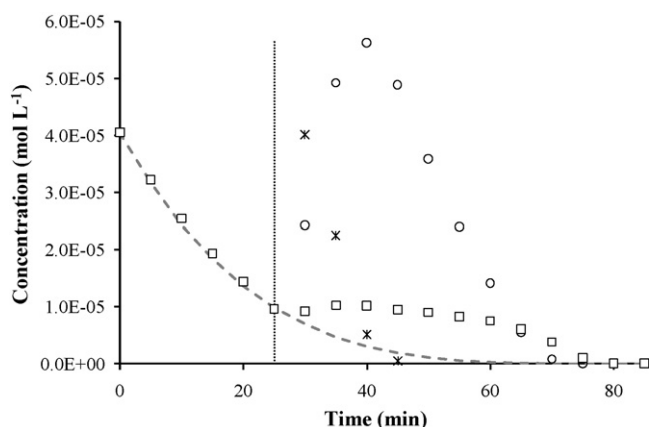


**Fig. 11.** Ethanol (*), ethanal (○) and propanone (□) concentration versus time during a multi-component photocatalysis reaction at 70 °C and 40% relative humidity. In this experiment, the lights were energized and the reactor was allowed to reach the set temperature prior to introducing the test compounds into the reaction loop. Propanone liquid was injected at 0 min, and ethanol liquid was injected at 25 min (horizontal dotted line). Ethanal is an intermediate produced during the photocatalytic degradation of ethanol. The dashed line represents the predicted concentration of propanone from time zero. As shown, propanone degradation is inhibited by the presence of ethanol and ethanal in this experiment.

configuration for this experiment was slightly different from the other experiments reported in this paper, so the kinetic data are not directly comparable. The catalyst formulation, a mixed oxide ($TiO_2/ZrO_2$) formulation, and specific reactor configuration for this experiment were presented in a previous publication [7]. In this experiment, the reaction temperature was 70 °C and the relative humidity was 40%. Titania and mixed oxide titania/zirconia photocatalyst materials are expected to exhibit similar surface properties.

A complicating factor in this experiment is the generation of a reaction by-product (ethanal, a.k.a.: acetaldehyde) from ethanol. As shown in Fig. 11, both ethanol and ethanal inhibit the degradation of propanone. Ethanol is observed to displace propanone on the catalyst surface as evidenced by the slight increase in gas phase propanone concentration. The by-product of ethanol PCO, ethanal, is immediately observed in the gas phase, and it starts to undergo photocatalytic oxidation as ethanol disappears. The gas phase propanone concentration decreases simultaneously with the decrease in ethanal, but it does not appear to undergo significant further oxidation until both the ethanol has been consumed and the aldehyde disappears. This is easily explained for ethanol due to its ability to hydrogen bond with the surface; however, it is again difficult to explain for the aldehyde. Ethanal has a smaller dipole moment and Henry's law constant than propanone, but a $k_{OH}$ that is much larger ($1.6 \times 10^{-11}$ cm$^3$ molecule$^{-1}$ s$^{-1}$ [27]). Based on this, propanone would be expected to outcompete, or at least compete favorably, with ethanal for surface sites; however, the opposite effect is observed. As discussed above with the propanone/propanal two-component experiment, polarity alone is not sufficient to explain the adsorption of this ketone to the catalyst surface.

Findings of this nature can have significant implications for applying photocatalysis in real-world situations where multiple compounds would most certainly be present. These results suggest that the ability to degrade any target analyte will be directly dependent on the presence of other compounds of similar or greater affinity for the catalyst surface, and/or chemical reactivity with species such as hydroxyl radical. It is critical, of course, to put in proper context the concentrations employed in this experiment (100 s of ppmv) and the concentrations expected in a real environment (sub-ppmv). In the limit of low concentration mixtures (ppbv or lower), one expects all species to simultaneously co-exist independently of each other on the catalyst surface. The site competition will be dominated by water and each species will react approximately at the same rate it would exhibit in a single component mixture at that absolute humidity. In the limit of high concentrations (10 s of ppmv or larger) we can expect that site competition will be dominated by the species with the strongest affinity for the hydrated surface. This implies that, for molecules of similar mass, alcohols would react first, followed by aldehydes, ketones, alkenes and alkanes. The intermediate case will be much more complex allowing for simultaneous adsorption of many species and requires more study to predict which, if any, interferences may exist. IAQ applications are closer to the lower limit for normal, non-problematic environments, so in normal building air one expects that individually measured rate constants at a given humidity can be used to accurately predict the performance of an air purification device; however, there are numerous industrial applications where competitive adsorption will be an important consideration for appropriately designing a PCO remediation system. For purposes of illustration, the concentrations used in this study were orders of magnitude higher than would be found in typical indoor air environments; however, they are representative of levels that might be found in industrial applications. Extrapolations would likely be required to apply these results to indoor air quality situations.

## 4. Conclusions

Results presented in this study demonstrate that at high concentrations (100 s of ppmv), C3 compounds have photocatalytic oxidation rates in the relative order 1-propanol > propanal > propanone > propene > propane. This is consistent with previously published rate data for some of these C3 compounds. The order of reaction rates can be partially explained by considering the intermolecular forces of attraction that exist between the gas-phase molecules and the hydrated (both physisorbed and chemisorbed water) titania surface, with the lone exception of the ketone. A model that incorporates Henry's law constant and hydroxyl radical reactivity was also applied and resulted in accurate predictions of the PCO reaction rate constants. It has been further shown that in mixtures of reacting species, a species with stronger binding energy to the photocatalyst surface can displace weaker-bound molecules and inhibit their further reaction until the stronger binding species has been sufficiently oxidized. Finally, it has been shown that by-products can interfere with the PCO of other molecules. Further investigation of binding energies of compounds of interest for PCO applications is clearly warranted through combinations of experimental techniques and atomistic modeling. This could enable a predictive capability for PCO rate constants that would enable scientists and engineers to build models capable of predicting the performance of air (and water) based photocatalytic purifiers.

## Acknowledgements

## References

[1] G.B. Raupp, C.T. Junio, Appl. Surf. Sci. 72 (1993) 321–327.
[2] W.A. Jacoby, M.R. Nimlos, D.M. Blake, R.D. Noble, C.A. Koval, Environ. Sci. Technol. 28 (1994) 1661–1668.
[3] X. Fu, W.A. Zeltner, M.A. Anderson, Appl. Catal. B: Environ. 6 (1995) 209–224.
[4] X. Fu, L.A. Clark, Q. Yang, M.A. Anderson, Environ. Sci. Technol. 30 (1996) 647–653.
[5] R.M. Alberici, W.E. Jardim, Appl. Catal. B: Environ. 14 (1997) 55–68.
[6] T.N. Obee, S.O. Hay, Environ. Sci. Technol. 31 (1997) 2034–2038.
[7] M.E. Zorn, D.T. Tompkins, W.A. Zeltner, M.A. Anderson, Environ. Sci. Technol. 34 (2000) 5206–5210.
[8] M.E. Zorn, D.T. Tompkins, W.A. Zeltner, M.A. Anderson, Appl. Catal. B: Environ. 23 (1999) 1–8.
[9] W. Doerffler, K. Kauffe, J. Catal. 3 (1964) 156–170.
[10] L. Amalric, C. Guillard, E. BlancBrude, P. Pichat, Water Res. 30 (1996) 1137–1142.
[11] R.J. Hall, J.J. Sangiovani, H.H. Hollick, T.N. Obee, S.O. Hay, Design of Air Purifiers for Aircraft Passenger Cabins Based on Photocatalytic Oxidation Technology, ASTM STP, No. 8251, 2000.
[12] P. Benfeld, R.J. Hall, T.N. Obee, S.O. Hay, J.J. Sangiovani, A Feasibility Study of Photocatalytic Air Purification for Commercial Passenger Airliners, United Technologies Research Center Internal Report, R97-1.300.9702, 1997.
[13] H. Courbon, M. Formenti, P. Pichat, J. Phys. Chem. 81 (1977) 550–554.
[14] T.N. Obee, S.O. Hay, J. Adv. Oxid. Technol. 4 (1999) 147–152.
[15] N. Takeda, T. Torimoto, H. Yoneyama, Bull. Chem. Soc. Jpn. 72 (1999) 1615–1621.
[16] R. Yang, Y.P. Zhang, Q.J. Xu, J.H. Mo, R.Y. Zhao, International Conference on Indoor Air Quality and Climate (Indoor Air 2005), Tsinghua University Press, Beijing, China, 2005.
[17] T.M. Twesme, D.T. Tompkins, M.A. Anderson, T.W. Root, Appl. Catal. B: Environ. 64 (2006) 153–160.
[18] M.L. Zhang, T.C. An, J.M. Fu, G.Y. Sheng, X.M. Wang, X.H. Hu, X.J. Ding, Chemosphere 64 (2006) 423–431.
[19] A.T. Hodgson, H. Destaillats, D.P. Sullivan, W.J. Fisk, Indoor Air 17 (2007) 305–316.
[20] A.L. Goodman, E.T. Bernard, V.H. Grassian, J. Phys. Chem. A 105 (2001) 6443–6457.
[21] M.I. Tejedor-Tejedor, F.M. Vichi, M.A. Anderson, J. Porous Mater. 12 (2005) 201–214.
[22] Q.Y. Xu, M.A. Anderson, J. Mater. Res. 6 (1991) 1073–1081.
[23] J. Barksdale, Titanium: Its Occurrence, Chemistry, and Technology, 2nd ed., Ronald Press Company, New York, 1966.
[24] J.D. Norris, Encyclopedia of Analytical Sciences, vol. 9, Academic Press, San Diego, 1995.
[25] N.B. Jackson, C.M. Wang, Z. Luo, J. Schwitzgebel, J.G. Ekerdt, J.R. Brock, A. Heller, J. Electrochem. Soc. 138 (1991) 3660–3664.
[26] C.G. Hill Jr., An Introduction to Chemical Engineering Kinetics and Reactor Design, Wiley, New York, 1977.
[27] R. Atkinson, Chem. Rev. 86 (1986) 69–201.
[28] CRC, Handbook of Chemistry and Physics, 71st ed., CRC Press, Boca Raton, FL, 1990.
[29] E. Wilhelm, R. Battino, R.J. Wilcock, Chem. Rev. 77 (1977) 219–262.
[30] R. Atkinson, D.L. Baulch, R.A. Cox, R.F. Hampson, J.A. Kerr, J. Troe. J. Phys. Chem. Ref. Data 18 (1989) 881–1097.
[31] D. Mackay, W.Y. Shiu, J. Phys. Chem. Ref. Data 10 (1981) 1175–1199.
[32] R.G. Buttery, L.C. Ling, D.G. Guadagni, J. Agric. Food Chem. 17 (1969) 385–389.
[33] M.G. Burnett, Anal. Chem. 35 (1963) 1567–1570.
[34] R. Atkinson, D.L. Baulch, R.A. Cox, R.F. Hampson, J.A. Kerr, M.J. Rossi, J. Troe. J. Phys. Chem. Ref. Data 26 (1997) 521–1101.